# Boundary Layer Losses in a Miniaturized Tapered Pulse Tube

**Ali Ghavami[1], Carl Kirkconnell[2] and S Mostafa Ghiaasiaan[1]**

[1]Georgia Institute of Technology,
G.W. Woodruff School of Mechanical Engineering
Atlanta, GA 30332, USA
[2]West Coast Solutions
Huntington Beach, CA 92647, USA

ABSTRACT

Miniaturized cryocoolers are a vital component for cooling of infrared sensors in small satellites. Cryocoolers operating at high frequencies (100-300 Hz range) can have smaller size since compression and expansion swept volumes reduce. Previously, we studied high frequency straight pulse tubes, and investigated the effects of diameter, aspect ratio of pulse tube, bounding temperatures and frequency on the boundary layer losses.

In this follow-up study the role of design parameters and operating conditions on the tapered pulse tube boundary layer losses is investigated. Computational fluid dynamics (CFD) is used for this investigation. The results show the existence of a size threshold, where smaller high frequency tapered pulse tube cryocoolers can no longer be useful due to their high boundary layer losses.

## INTRODUCTION

There is growing interest in more capable small satellite payloads as small satellites become more mature and low earth orbit becomes increasingly commercialized. Infrared (IR) sensors are one of the most important components of recently developed small satellites. IR sensors can be used for imaging of planetary bodies, among other applications. These IR sensors need to be cooled down by miniature cryocooler for the sake of taking better pictures with little noise. Cryocooler miniaturization requires application of state of art technology because of its minimal volume and weight to address the cooling requirements for IR sensors.

Pulse Tube (PT) miniaturization has been studied extensively. The combination of high efficiency, which they share with Stirling coolers, and lack of cold end moving parts makes pulse tube refrigerators especially promising as miniature cryocoolers. Among past investigators, Liang et al [1] developed a coaxial PT with an outer diameter of 9 mm and cooling capacity of 200 mW at 81K at a frequency of 50 Hz. Tward et al [2] developed a similar pulse tube cooler cooling at 65K with 80 Hz, and Chen et al [3] reached 50K by two compact integrated coaxial miniature pulse tubes.

There is a size threshold for PT coolers below which they are no longer efficient at small sizes especially at high frequencies. High frequency is essential for small cryocoolers since high frequency makes the compression and expansion swept volume smaller, which in turn leads to

*Cryocoolers 21,* edited by R.G. Ross, Jr., J.R. Raab and S.D. Miller

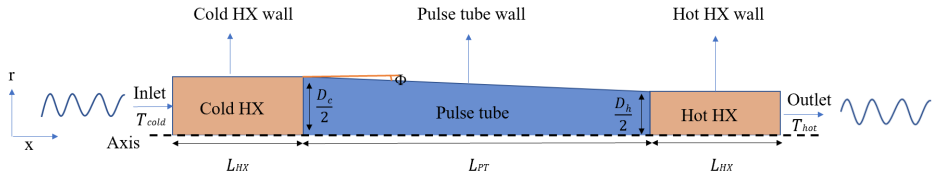


**Figure 1.** Computational domain with boundary conditions.

**Table 1.** Model parameters.

| Model parameter | Value |
|---|---|
| Working gas | Helium |
| Frequency (f) | Varies between 175 – 300 Hz (sinusoid) |
| Cold end temperature ($T_{cold}$) | 80 K |
| Hot end temperature ($T_{hot}$) | 300 K |
| Mean pressure ($P_{mean}$) | 1.59 MPa |
| Cold and hot mass flow rate phase angle (θ) | 30° cold end leading |
| Pulse tube diameter at warm end ($D_h$) | 1, 4, 7 mm |
| Pulse tube diameter at cold end (Dc) | Derived from pulse tube length and tapered angle |
| Pulse tube tapered angle (Φ) | Varies between 0 –5 degree |
| Pulse tube aspect ratio ($L_{PT}/D_h$) | 10 |
| Pulse tube length ($L_{PT}$) | Derived based on aspect ratio |
| Heat exchanger lengths ($L_{HX}$) | 0.3 $L_{PT}$ |
| Heat exchanger viscous resistance | $7.435\times10^{8}$ $m^{-2}$ |
| Heat exchanger inertial resistance | 8147 $m^{-1}$ |
| Heat exchanger porosity | 0.68 |

smaller size actuators and other components of the cooler. Previous studies by this research group [4] shows that the enthalpy transport capacity of a PT drastically diminishes as pulse tube diameter shrinks from 10 mm to 1 mm due to boundary layer losses. Ghavami et al [5] performed a sensitivity analysis on the straight PT and the size threshold below which boundary layer losses become dominant. This Computational Fluid Dynamic (CFD) study is a follow up of the previous works [4, 5] and is meant to investigate the effect of tapering of a PT on the boundary layer losses. The effect of working frequency and tapered angle on boundary layer losses is investigated for various PT diameters. A goal is to find the size threshold below which a PT is no longer efficient at high frequency and small size. Below such a size threshold, miniature Stirling cryocoolers demonstrate better functionality at high frequencies [6-8]. The main goal of this research is to see if the scope of applicability for a PT relative to a Stirling can be extended with tapering. It is noted that this study focuses only on the boundary layer losses in a pulse tube itself and not the other components of a cryocooler.

## GEOMETRIC CONFIGURATIONS AND MODEL ASSUMPTIONS

Figure 1 summarizes the computational domain and its boundary conditions, and Table 1 depicts the model parameters. These parameters are in accordance with past studies [4, 5] and are meant to make the results comparable.

The frequency varies between 175 to 300 Hz. The bounding temperatures are fixed and are set to 300K for the hot end, and 80 K for the cold end which is the temperature at low earth orbit. The diameter of the hot end of the pulse tube ($D_h$) is reduced in steps from 7mm to 1mm to examine the effect of miniaturization, while tapering at specified angles is imposed. The aspect ratio, defined based on the diameter at the hot end, for all cases is set to 10.

The cold and hot ends of the pulse tubes are typically connected to a cold and hot heat exchanger, respectively, where the heat exchangers are porous media structures. In the

simulations, these heat exchangers are modeled as porous media zones with arbitrary structures but known hydrodynamic characteristics. It is also assumed that these porous zones make the incoming flow to the pulse tube isothermal and uniform. The diameter of each heat exchanger is equal to its corresponding pulse tube end and the lengths of heat exchangers are equal to 0.3 of pulse tube length. Modeling of heat exchanger requires specifying viscous and inertial loss terms. The heat exchanger viscous and inertial resistances are set to $7.435\times10^{8}$ $m^{-2}$ and 8147 $m^{-1}$ respectively. The porosity is also assumed to be 0.68. These numbers tie back to our prior assumptions for the straight pulse tubes. All these parameters remain constant for all cases.

The analysis is 2D axisymmetric and the pulse tube wall is assumed to be adiabatic. The inlet and outlet of the computational domain are subject to oscillating mass flow rates where the cold end mass flow rate is leading by 30 degrees to represent the typical phase lag between the two ends of PTs. This phase shift between cold and hot end mass flow rates is fixed for all cases. The details of mass flow rate will be discussed in the next section.

## THEORY AND METHOD OF SOLUTION

The conservation equations including continuity, momentum in axial direction, momentum in radial direction and energy equations for 2D axisymmetric flow are:

$$\frac{\partial \rho}{\partial t}+\frac{\partial(\rho u)}{\partial x}+\frac{1}{r}\frac{\partial(r\rho v)}{\partial r}=0 \tag{1}$$

$$\frac{\partial}{\partial t}(\rho u)+\frac{1}{r}\frac{\partial(r\rho uv)}{\partial x}+\frac{1}{r}\frac{\partial(r\rho uv)}{\partial r}=-\frac{\partial P}{\partial x}+\frac{1}{r}\frac{\partial}{\partial x}\left[r\mu\left(2\frac{\partial v}{\partial x}-\frac{2}{3}(\nabla.\vec{V})\right)\right]+\frac{1}{r}\frac{\partial}{\partial r}\left[r\mu\left(\frac{\partial u}{\partial r}+\frac{\partial v}{\partial x}\right)\right] \tag{2}$$

$$\frac{\partial}{\partial t}(\rho v)+\frac{1}{r}\frac{\partial(r\rho uv)}{\partial x}+\frac{1}{r}\frac{\partial(r\rho uv)}{\partial r}=-\frac{\partial P}{\partial r}+\frac{1}{r}\frac{\partial}{\partial x}\left[r\mu\left(\frac{\partial v}{\partial x}+\frac{\partial u}{\partial r}\right)\right]+\frac{1}{r}\frac{\partial}{\partial r}\left[r\mu\left(2\frac{\partial v}{\partial r}-\frac{2}{3}(\nabla.\vec{V})\right)\right]-2\mu\frac{v}{r^2}+\frac{2}{3}\frac{\mu}{r}(\nabla.\vec{V}) \tag{3}$$

$$\rho c\left(\frac{\partial T}{\partial t}+u\frac{\partial T}{\partial x}+v\frac{\partial T}{\partial r}\right)=\frac{1}{r}\frac{\partial}{\partial r}\left(rk\frac{\partial T}{\partial r}\right)+\frac{\partial}{\partial x}\left(k\frac{\partial T}{\partial x}\right)2\mu\left[\left(\frac{\partial v}{\partial r}\right)^2+\left(\frac{v}{r}\right)^2+\left(\frac{\partial u}{\partial x}\right)^2+\frac{1}{2}\left(\frac{\partial v}{\partial x}+\frac{\partial u}{\partial r}\right)^2-\frac{1}{3}(\nabla.\vec{V})^2\right] \tag{4}$$

where μ, ρ, c, and k are dynamic viscosity, density, specific heat, and conductivity of the fluid, respectively, u is the velocity in the axial direction and v represents the velocity component in radial direction.

All fluid properties are extracted from Engineering Equation Solver software (EES) [9]. Temperature dependent variables at $P_{mean}$ for the range of temperatures between 80-300K are extracted from EES. For easier implementation, polynomial regression is fitted to these data and the results for density, dynamic viscosity, heat capacity and thermal conductivity are as follows:

$$\rho\left(\frac{kg}{m^3}\right)=-2\times10^{-6}T^3+0.0013T^2-0.2944T+25.43 \tag{5}$$

$$\mu\left(\frac{kg}{m.s}\right)=5\times10^{-8}T+4\times10^{-6} \tag{6}$$

$$c\left(\frac{kJ}{kg.K}\right)=-3\times10^{-8}T^3+2\times10^{-5}T^2-0.0041T+5.459 \tag{7}$$

$$k\left(\frac{W}{m.K}\right)=0.0004T+0.0313 \tag{8}$$

The mass flow rate amplitude applied at both ends are normalized by the pulse tube size in a way that the gas displacement at each of the cold and hot ends is equal to 25% of the total pulse tube size, which is a common assumption in pulse tube cryocoolers. This can be shown mathematically as [5]:

$$V_{PT}=\frac{1}{12}\pi L_{PT}(D_c^2+D_cD_h+D_h^2) \tag{9}$$

$$dV=dV_c=dV_h=0.25V_{PT} \tag{10}$$

$$dM_c=\frac{dV\times P_{mean}}{R\times T_{cold}},\qquad dM_h=\frac{dV\times P_{mean}}{R\times T_{hot}} \tag{11}$$

$$|\dot{m}_{cold}|=\sqrt{2}\frac{dM_c}{dt}=\sqrt{2}\times dM_c\times 2f,\qquad |\dot{m}_{hot}|=\sqrt{2}\frac{dM_h}{dt}=\sqrt{2}\times dM_h\times 2f \tag{12}$$

where R is the ideal gas constant for the working fluid (Helium in this case).

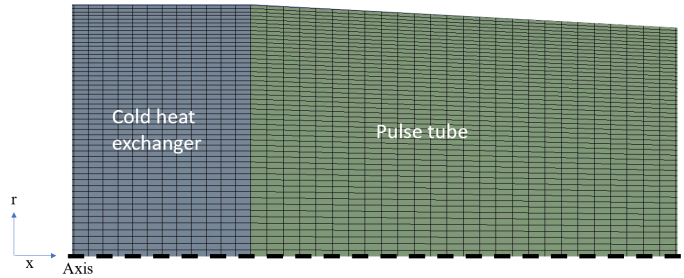


**Figure 2.** Mesh generation on the portion of tapered pulse tube and the cold heat exchanger.

To address the effect of miniaturization, the pulse tube efficiency is defined as the ratio of cycle averaged total enthalpy flux, $<\dot{H}>$, divided by the total input PV power. The cycle average total enthalpy flux, input PV power, and the PT efficiency, $\eta$, can be calculated from:

$$<\dot{H}> = \frac{\int_{cycle}\left(\int_0^{D/2}\rho u\left(h+\frac{1}{2}|u|^2\right)2\pi r dr\right)dt}{t_{cycle}} \tag{13}$$

$$<P\dot{V}> = \frac{1}{2}RT_{cold}\left(\frac{P_{amp}}{P_{mean}}\right)|\dot{m}_{cold}|\cos\theta \tag{14}$$

$$\eta = \frac{<\dot{H}>}{<P\dot{V}>} \tag{15}$$

where $t_{cycle}$ is cycle period time, u is axial velocity, and $P_{amp}$ is pressure amplitude ($P_{max} - P_{mean}$) in the pulse tube.

## NUMERICAL SOLUTION PROCEDURES

Equations 1 through 8 are solved by the aid of ANSYS Fluent [10]. The oscillating mass flow rates at the inlet and outlet are provided through a user define function (UDF) in Fluent. The UDF file is developed in C++ [11]. These mass flow rates can be formulated as follows where $|\dot{m}_{cold}|$ and $|\dot{m}_{hot}|$ are calculated from equation 12.

$$\dot{m}_{inlet} = |\dot{m}_{cold}|\sin(2\pi ft), \quad \dot{m}_{outlet} = |\dot{m}_{hot}|\sin(2\pi ft - \theta) \tag{16}$$

Figure 2 displays the computational mesh. The total number of elements in axial direction is set to 700 elements where 500 of them are dedicated to tapered pulse tube and 100 elements to each heat exchanger. In radial direction, the total number of elements is set to 50 with a bias factor of 2. This bias factor makes the mesh finer near the wall in comparison to the centerline meshes by factor 2. Grid independence was investigated by increasing the number the of elements and calculating the cycle average total enthalpy transport rate between the two ends of the pulse tube under steady-periodic conditions. Generating finer mesh in the computational domain only changed the cycle averaged enthalpy transport rate by a maximum of 0.5% which confirmed the simulation results were essentially grid independent.

The simulations are transient, two-dimensional and axisymmetric. The flow is laminar and temperature dependent properties based on equations 5-8 are used. Constant temperatures of 80K and 300K are set at the cold and hot exchangers, respectively. The mean pressure is set to 1.59MPa. The SIMPLE algorithm is chosen for solving pressure-velocity coupling. Finite volume technique is implemented for solving the equations. For equation discretization, the least squares method for gradients, the standard second order method for pressure, and second order upwind scheme for momentum and energy equations are selected. First order implicit is used for transient formulation. The under-relaxation factor for pressure and momentum is set to 0.3 and 0.75 respectively. For convergence criteria, the residual is set to $10^{-5}$ for continuity and momentum equations, and $10^{-12}$ for energy equation. It is assumed that each cycle consists of 100 time steps which results in time steps equal to $1.66\times10^{-5}$ seconds for 300Hz frequency. Post processing of the results is performed by the aid of MATLAB [12] and Tecplot [13].

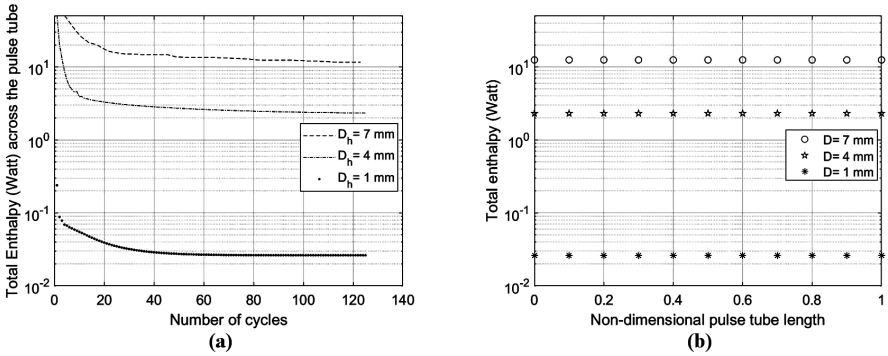


**Figure 3.** Convergence of results for f = 300Hz, (a) the effect of number of cycles on convergence of cycle average total enthalpy flux at the middle of the pulse tube, (b) cycle average total enthalpy flux throughout the length of the pulse tube at steady periodic conditions ($100^{th}$ cycle).

## RESULTS AND DISCUSSION

Cycle average total enthalpy flux at the middle of the pulse tube is calculated to track reaching periodic steady state solution. The periodic steady state is a condition where cycle average characteristics of flow no longer change from one cycle to the next. It is shown in Figure 3a that periodic steady state condition is reached after about 100 cycles by tracking cycle average total enthalpy flux at the middle of the pulse tube. All simulations run for 125 cycle to ensure converged periodic steady state.

Figure 3b also illustrates the convergence solution by showing constant total enthalpy flux all across the length of the pulse tube. The total enthalpy fluxes at different axial positions of the pulse tube should be equal to each other since adiabatic or zero heat flux boundary condition is applied at the wall of the pulse tube. The axial position of the pulse tube is nondimensionalized by the length of pulse tube, $L_{PT}$.

Figure 4 illustrates the effect of tapering on the boundary layer losses for the miniature PT. Temperature contours for straight and 5-degree tapered pulse tubes are depicted at different snapshots during a cycle for f=300 Hz and $D_h$= 1 mm. The left axis is for a straight PT, while the right axis represents the

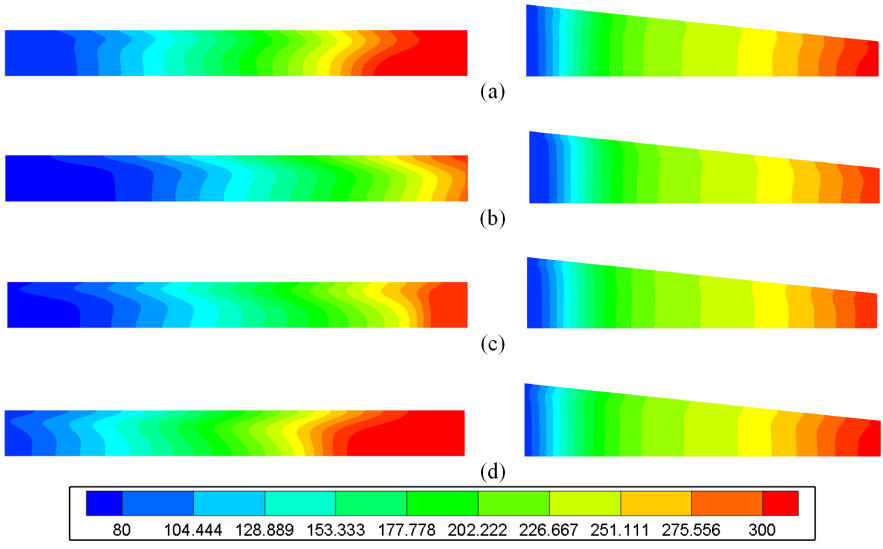


**Figure 4.** Temperature contour plots of straight (left column) and 5 degree tapered (right column) pulse tube for $D_h$ = 1mm and f= 300Hz at different cycle time, (a) 1/4 cycle, (b) 2/4 cycle, (c) 3/4 cycle, (d) 4/4 cycle.

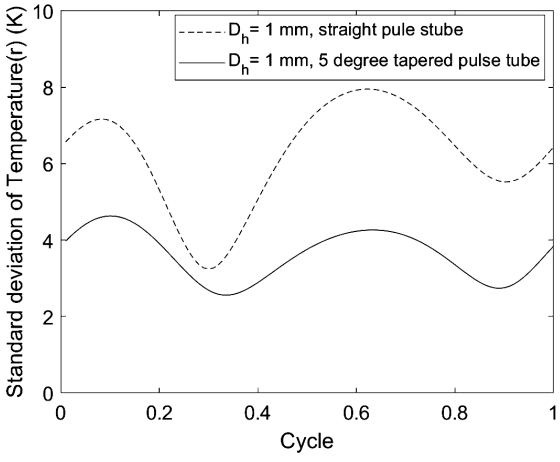


**Figure 5.** Standard deviation of the distribution of temperature over the cross-section of the pulse tube for $D_h = 1$ mm, $f = 300$ Hz, and aspect ratio of 10 at the middle of pulse tube ($L_{PT}/2$).

corresponding tapered pulse tube at the same snapshot in the cycle. The aspect ratio ($L_{PT}/D_h$) in the main computational domain is 10 for all cases but this aspect ratio is divided by two in Figure 4 for better visualization of the contour plots. The top edge is a wall and the bottom edge is the axis of symmetry. As can be seen in Figure 4, the flow mixing in axial direction and temperature variation in the radial direction are significantly stronger in the straight pulse tube in comparison to the tapered pulse tube. The deviation from 1-D distribution of temperature in pulse tube leads to enthalpy loss and reduction of the efficiency. The tapered pulse tube has lower boundary losses in comparison to the corresponding straight version due to less steep temperature gradient in the flow direction. This is shown in Figure 5 quantitively by plotting the standard deviation (SD) of fluid temperature over the cross section of the pulse tube at the middle of the axial position during a full one cycle. The straight pulse tube has higher standard deviation at all time steps which indicated higher boundary layer losses.

Figure 6 compares the dependence of the boundary layer losses on frequency and diameter for the straight and 5-degree tapered pulse tubes. The frequency varies from 175 to 300 Hz and the pulse tube diameter at the hot end varies from 7 to 1 mm. Frequency has a small effect on the PT boundary layer losses and the efficiency decreases as the frequency increases for all cases. Reducing the hot end diameter

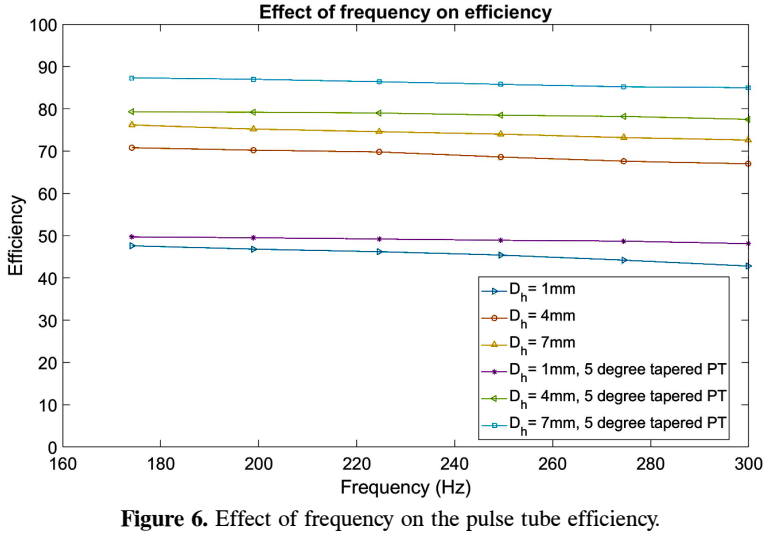


**Figure 6.** Effect of frequency on the pulse tube efficiency.

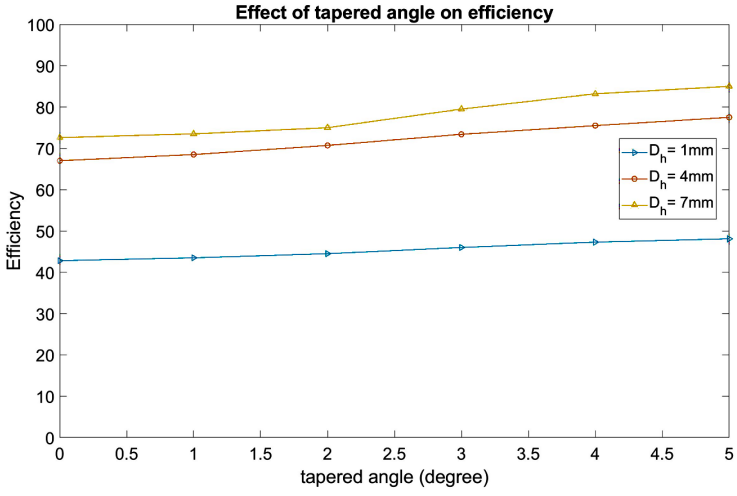


**Figure 7.** Effect of tapered angle on the pulse tube efficiency

from 7 to 1 mm drastically reduces the efficiency which shows a greater effect of boundary layer losses as the PT diameter becomes smaller. However, it can be seen from Figure 6 that tapering the pulse tube can reduce the boundary layer losses and improve the efficiency. The improvement in efficiency due to tapering is greater for larger pulse tube diameters. Comparing the two corresponding straight and tapered pulse tube at the same diameter shows higher improvement at higher frequencies. This phenomenon can be more clearly seen by comparing the plots for $D_h$=1mm in Figure 6.

Figure 7 illustrates the effect of tapered angle on the pulse tube efficiency at the constant frequency of 300Hz. The tapering angle is changed from 1 to 5 degrees. The pulse tube efficiency is gradually increased as the tapering angle increases. However, this improvement in efficiency is greater at larger diameters.

## CONCLUSION

Two-dimensional axisymmetric CFD simulations were performed for straight and tapered pulse tubes to investigate the effect of tapering on boundary layer losses for miniaturized pulse tubes. The study is performed for frequencies 75 to 300 Hz, tapering angles from 0 to 5 degrees, and diameters ranging from and 7 to 1 mm. It was shown that the total enthalpy flux losses across the length of the pulse tube drastically increases as the diameter becomes smaller due to the deviation from 1-D temperature distribution as well as the increase in the boundary layer effect. These results confirm that the pulse tube cryocooler may not be a good option for highly miniaturized cryocoolers working at high frequency. It was also shown that tapering the pulse tube reduces the boundary layer losses, however, and this improvement is greater for pulse tubes with larger diameters operating at higher frequencies.

## ACKNOWLEDGMENT

This work was funded by West Coast Solutions (wecoso.com) through the WCS-GT Cryocooler Research Fund.

## REFERENCES

1. J. Liang, Y. Zhou, W. Zhu, W. Sun, J. Yang, and S. Li, “Study on miniature pulse tube cryocooler for space application,” *Cryogenics,* vol. 40, no. 3 (2000), pp. 229-233.

2. E. Tward, T. Nguyen, J. Godden, and G. Toma, “Miniature pulse tube cooler,” *AIP Conference Proceedings*, 2004, vol. 710, no. 1: American Institute of Physics, pp. 1326-1329.

3. H. Chen, L. Yang, J. Cai, J. Liang, L. Zhang, and Y. Zhou, “An Integrated Miniature Pulse Tube Cryocooler at 80K,” *AIP Conference Proceedings*, 2008, vol. 985, no. 1: American Institute of Physics, pp. 673-677.

4. C. Kirkconnell, A. Ghavami, S. M. Ghiaasiaan, and M. Perrella, "Role of size on the relative importance of fluid dynamic losses in linear cryocoolers," *IOP Conference Series: Materials Science and Engineering*, 2017, vol. 278, no. 1: IOP Publishing, p. 012173.

5. A. Ghavami, C. Kirkconnell, and S. M. Ghiaasiaan, "Sensitivity analysis on miniaturize pulse tube boundary layer losses," *IOP Conference Series: Materials Science and Engineering*, 2020, vol. 755, no. 1: IOP Publishing, p. 012014.

6. R. Arts *et al.*, "Miniature Stirling cryocoolers at Thales Cryogenics: Qualification results and integration solutions," in *Tri-Technology Device Refrigeration (TTDR)*, 2016, vol. 9821: International Society for Optics and Photonics, p. 98210P.

7. C. Kirkconnell, A. Ghavami, and S. Ghiaasiaan, "Computational fluid dynamics study of displacer shuttle loss in miniature Stirling cryocoolers," *Tri-Technology Device Refrigeration (TTDR) III*, 2018, vol. 10626: International Society for Optics and Photonics, p. 1062604.

8. T. Nast *et al.*, "Development of Microcryocoolers for Space and Avionics Applications," *Cryocoolers 19,* ICC Press, Golden CO (2016), pp. 65-74.

9. S. Klein and S. Alvarda, "Engineering equation solver (EES)," ed: F-chart software, WI, 2007.

10. A. Fluent, "14.5 user's guide," *Fluent Inc., Lebanon, NH,* 2011.

11. H. Schildt, *C++: The complete reference*. McGraw-Hill/Osborne, 2003.

12. D. J. Higham and N. J. Higham, *MATLAB guide*. SIAM, 2016.

13. W. Bellevue, "Tecplot. 360 2010 User's Manual," ed: Tecplot, Inc, 2010.